Vol 457|1 January 2009|doi:10.1038/nature07650

LETTERS

Seismic evidence for overpressured subducted oceanic crust and megathrust fault sealing

Pascal Audet[1]†, Michael G. Bostock[1], Nikolas I. Christensen[1,2] & Simon M. Peacock[1]

Water and hydrous minerals play a key part in geodynamic processes at subduction zones[1–3] by weakening the plate boundary, aiding slip and permitting subduction—and indeed plate tectonics—to occur[4]. The seismological signature of water within the forearc mantle wedge is evident in anomalies with low seismic shear velocity marking serpentinization[5–7]. However, seismological observations bearing on the presence of water within the subducting plate itself are less well documented. Here we use converted teleseismic waves to obtain observations of anomalously high Poisson's ratios within the subducted oceanic crust from the Cascadia continental margin to its intersection with forearc mantle. On the basis of pressure, temperature and compositional considerations, the elevated Poisson's ratios indicate that water is pervasively present in fluid form at pore pressures near lithostatic values. Combined with observations of a strong negative velocity contrast at the top of the oceanic crust, our results imply that the megathrust is a low-permeability boundary. The transition from a low- to high-permeability plate interface downdip into the mantle wedge is explained by hydrofracturing of the seal by volume changes across the interface caused by the onset of crustal eclogitization and mantle serpentinization. These results may have important implications for our understanding of seismogenesis, subduction zone structure and the mechanism of episodic tremor and slip.

In recent years, it has become increasingly apparent that large quantities of water (H_2O) are stored in the mantle wedge as the serpentine mineral antigorite[5]. Compelling evidence for the presence of antigorite comes from seismic observations that reveal the presence of highly resolved, low-shear-velocity anomalies in both warm (young slab, for example Cascadia[6]) and cold (old slab, for example northeast Japan[7]) subduction zone environments in locations predicted by thermal and petrological models[5]. Water in the mantle wedge most probably originates from the dehydration of hydrous minerals within subducting oceanic crust and mantle, which will occur at shallower depths (<50 km) in warmer environments[1,3]. Hydrous minerals form within oceanic lithosphere (1–2% H_2O in the crust[1]) as a result of hydrothermal circulation and alteration at spreading ridges, along fracture zones, and in the region of the trench and outer rise. There is little constraint, however, on the *in-situ* abundance and distribution of H_2O in the fluid and hydrous minerals within subducting oceanic crust, even though this knowledge is likely to be important in assessing the strength of the plate interface and nature of seismogenesis. Recent studies of episodic tremor and slip (ETS) in both Cascadia and Japan point to an origin that involves, either directly or indirectly, fluids near the plate boundary, downdip of the locked zone but updip of its intersection with forearc mantle[8–10]. Characterizing the physical state of subducted oceanic crust and distribution of fluids therein may help in understanding the temporal and spatial occurrence of ETS events.

We use observations of converted teleseismic waves (or receiver functions) recorded over a POLARIS portable array of seismometers across Vancouver Island at spacings of approximately 10 km (Fig. 1). All receiver functions from this experiment are plotted in raw form from west-southwest to east-northeast according to station position and, for individual stations, according to their sampling points (Fig. 2a). These data are sensitive to structures with scale lengths of 1–10 km and are dominated across the entire profile by the signature of an eastward-dipping low-velocity zone. This signature includes three sets of oppositely polarized pulses comprising forward-scattered P-to-S (Ps, 3–4 s at station PGC) conversions, and back-scattered P-to-S (Pps, 13–15 s at PGC) and S-to-S (Pss, 17–20 s at PGC) conversions afforded by reflection of the teleseismic wavefield at the Earth's free surface. These signals coincide with prominent, dipping seismic reflectors and have been previously interpreted to represent oceanic crust of the subducting Juan de Fuca plate[11], consistent with its expression in studies further south beneath Oregon[5] and worldwide[6,12,13].

Here we re-examine the signature of the different scattered modes in more detail. It is widely appreciated[14,15] that the timing (relative to the incident P-wave arrival, time 0 in Fig. 2a) of the scattered modes from a given interface can be used to constrain both depth and average

Figure 1 | Geographical map of northern Cascadia subduction zone. Location of the three-component, broadband seismic stations that recorded data used in this study are shown as inverted red triangles. The deformation front is indicated by the thin solid black line. Note that the array is oriented approximately perpendicular to the strike of subduction, which trends N45°W.

[1]Department of Earth and Ocean Sciences, University of British Columbia, Vancouver, British Columbia V6T 1Z4, Canada. [2]Department of Geology and Geophysics, University of Wisconsin-Madison, 1215 West Dayton Street, Madison, Wisconsin 53706, USA. †Present address: Seismological Laboratory, University of California Berkeley, 215 McCone Hall, Berkeley, California 94720, USA.

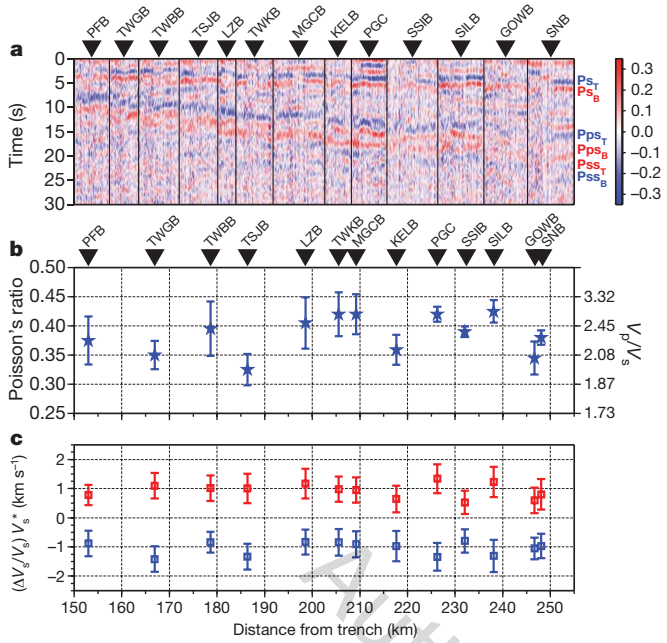

Figure 2 | Radial receiver function results beneath northern Cascadia. **a**, Receiver function results for all data filtered between 0.05 and 0.5 Hz used in the analysis sorted by station position along the array and, for each station, by back-azimuth of incident wavefield. Amplitudes are relative to incident P-wave. Red and blue colours correspond to velocity increase and decrease with depth, respectively. Forward- (Ps) and back-scattered (Pps and Pss) phases show oppositely polarized pulses that are manifest of waves converted from the top and bottom boundaries of a dipping, low-velocity layer, indicated by blue and red labels. **b**, Estimated V_P/V_S and Poisson's ratios for the low-velocity layer. Errors are standard deviations from bootstrap estimates. Elevated values (~0.4) are interpreted as near-lithostatic pore-fluid pressures. **c**, S-velocity perturbations relative to a one-dimensional reference model (V_S*) using a Born approximation for radial Ps phases. Error bars are one standard deviation. Positive (red) and negative (blue) velocity contrasts from the bottom and top, respectively, of the low-velocity layer are of similar amplitude.

P-to-S velocity ratio (V_P/V_S) of the overlying column. It can also be shown (see Supplementary Information) that relative times between two arrivals from distinct boundaries within the lithospheric column for each set of scattered modes can be used similarly to characterize the interval properties between the two boundaries, largely independent of overlying structure, even for dipping layers.

This recognition allows us to investigate the velocity structure (that is, V_P/V_S) of the downgoing oceanic crust. The key constraint is the ratio of the direct conversion delay time (ΔT_{Ps}, the difference in time between direct conversions from the top and bottom of the oceanic crust) to the corresponding back-scattered quantities (ΔT_{Pps}, ΔT_{Pss}). In the two extremes as V_P/V_S tends to 1 and ∞, ΔT_{Ps} will tend to 0 and ΔT_{Pps} ($\Delta T_{Pss}/2$), respectively. Care must be taken in measuring these quantities, because low-pass filtering at corner periods greater than twice the true separation between pulses will bias measurements of ΔT_{Ps}, ΔT_{Pps} and ΔT_{Pss} to greater values (see Supplementary Information).

Figure 2b shows our estimates of oceanic crustal V_P/V_S beneath each station of the array. These estimates are extremely high and it becomes more practical to speak in terms of Poisson's ratio (σ, for which there is an upper bound of 0.5 for inviscid fluids) around 0.4. These values cannot be due to compositional effects (that is, mineralogy within the downgoing oceanic crust). The common oceanic crustal rocks basalt, diabase and gabbro have σ between 0.28 and 0.29. At the prevailing temperatures and pressures (~1 GPa, ~500 C), these rocks will have been metamorphosed to upper amphibolite facies leading to a drop in σ to 0.26 or 0.27 (ref. 16). Antigorite, the high-temperature variety of serpentine, has a σ of 0.29 (ref. 17). Even the most extreme candidates, the low-pressure serpentine minerals chrysotile and lizardite[16], have σ below 0.37, and their presence can be further ruled out on the basis of pressure, temperature and compositional considerations[18]. The only plausible explanation is that of high pore-fluid pressures. Widely documented high pore-fluid pressures existing at shallower levels in accretionary prisms are due primarily to porosity reduction[19] but it is more likely that our observations indicate mineral dehydration[20]. Unfortunately, a precise correspondence between σ and pore-fluid pressure is hampered by the lack of laboratory measurements at confining pressures corresponding to 20–40 km depth. Nonetheless, extrapolation of measurements made at lesser pressures[20] shows that it is it likely that the oceanic crust beneath Vancouver Island is overpressured (near lithostatic), a result with a range of important implications.

Evidence for high pore-fluid pressure in the Nankai subduction zone has been presented recently[9,21] but these studies, using different forms of travel-time tomography, have found less extreme values of V_P/V_S. Measurements of V_P/V_S derived from tomography are likely to be biased towards normal values through the blurring effects of regularization, simultaneous earthquake relocation and the inherent difficulties in imaging low-velocity zones with travel times[22,23]. Estimates of σ obtained using scattered waves are likely to be better resolved owing to their greater sensitivity to local velocity changes.

Our documentation of high pore-fluid pressure implies that the plate interface probably represents a low-permeability boundary. Using Darcy's law, we estimate the permeability of the interface to be $\sim 5 \times 10^{-25}$ to $\sim 5 \times 10^{-22}$ m^2, assuming pore-fluid pressures equal to lithostatic pressures beneath the interface, a 0.65-GPa pressure drop across the interface corresponding to hydrostatic pore-fluid pressure above the interface at a depth of 35 km, a slab fluid production rate of 10^{-4} m^3 (m^2 yr)$^{-1}$ (ref. 5), an interface thickness of 1 to 1,000 m, and a dynamic viscosity of 10^{-4} Pa s for H_2O at 500 C and 1 GPa. These estimates are lower than measurements of basaltic oceanic basement permeabilities in the range 10^{-21} to 10^{-11} m^2 made at length scales of 1 to 1,000 m (ref. 24). The significance of our estimate is reinforced by noting that the greatest permeabilities are found within the upper few hundred metres of oceanic crust and increase with scale length[24]. The low permeability of the plate interface may reflect deformation-induced grain-size reduction[25] or the precipitation of minerals from migrating fluids[26,27].

Further evidence supporting a low-permeability plate boundary at crustal levels stems from scattered wave amplitudes that are sensitive to velocity contrasts at interfaces (Fig. 2c). Amplitudes of arrivals for a given scattering mode originating from the bottom and top oceanic crustal boundaries are comparable, indicating similar S-velocity jumps of ± 1 km s^{-1}, respectively. The lower boundary jump is consistent with that expected for the oceanic Moho which marks the juxtaposition of lower-velocity gabbro with higher-velocity mantle peridotite. The lower crust of the overriding plate is thought to be formed of dominantly mafic accreted terranes[28] and would thus be expected to afford little or no contrast in seismic velocity with oceanic crust. Prominent amplitudes of scattered waves from the upper boundary thus support a sharp contrast from low-velocity oceanic crust containing trapped fluids to higher velocity overriding crust characterized by much lower pore-fluid pressure.

Low permeability of the plate boundary at depths less than 35 km contrasts with the seismic expression of forearc mantle serpentinization, which appears downdip at depths greater than 40 km in this region[5,11] and suggests that H_2O is readily transported into the wedge (Fig. 3). A change in the nature of the plate boundary seal can be explained by the large (>10%) volume reduction and release of H_2O that accompanies eclogitization[29], the last significant metamorphic facies transition experienced by oceanic crust. Both this reaction and the still greater volume expansion accompanying serpentinization of the mantle wedge[30] could be expected to increase permeability near the plate boundary through fracture generation. This interpretation is consistent with the seismic signature in the cold subduction zone

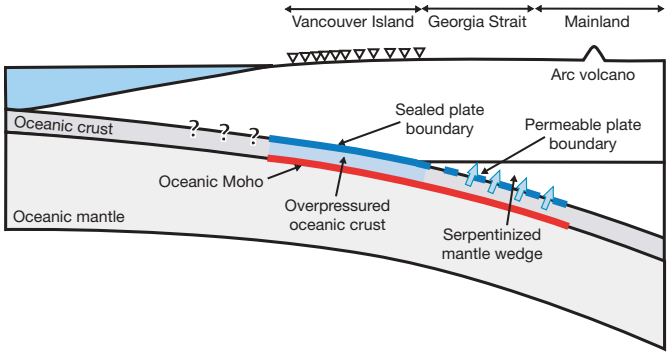

Figure 3 | Schematic interpretation of receiver function results. Updip limit of overpressured oceanic crust is unconstrained. Note vertical exaggeration.

setting of northeast Japan, where a serpentinite layer is interpreted to form above subducting oceanic crust at onset of eclogitization near ~90 km depth[6].

It is worth noting that in warm subduction zones, ETS tends to occur in the vicinity of the plate interface near but seaward of the wedge corner[8,9]. Our documentation of high pore-fluid pressures in this region supports two groups of models that involve fluids: (1) ETS is triggered by hydrofracturing at the plate interface[10]; and (2) ETS occurs where high pore-fluid pressures extend the region of conditionally stable slip[9,21]. A downdip change in permeability across the plate interface could be explained by hydrofracturing of the seal where hydraulic conductivities become sufficiently high near the onset of eclogitization. Moreover, it might represent an important factor in altering the mode of slip along the thrust within the frictional stability transition zone. Our model suggests the possibility of linking the recurrence of ETS at regular time intervals to periodic cycles of steady pore-fluid pressure build-up from dehydration of subducted oceanic crust, fluid release from fracturing of the interface during ETS, and subsequent precipitation sealing of the plate boundary.

Finally, our documentation of high pore-fluid pressure in the subducting plate has important implications for the interpretation of tomographic velocity images, and the position of the plate boundary interface. High pore-fluid pressures result not only in elevated σ (and V_P/V_S) but also in depressed absolute velocities (−20% and −30% for P-waves and S-waves, respectively, in the measurements of Christensen[16]). Consequently, identification of a tomographic isovelocity contour that does not account for this effect, as proxy for the oceanic Moho[28], will yield interface depths that are significantly overestimated[11].

Received 20 May; accepted 17 November 2008.

1. Peacock, S. M. Fluid processes in subduction zones. *Science* **248,** 329–337 (1990).
2. Stern, R. J. Subduction zones. *Rev. Geophys.* **40,** doi:10.1029/2001RG000108 (2002).
3. Kirby, S. H., Engdahl, E. R. & Denlinger, R. in *Subduction Top to Bottom* (eds Bebout, G. E., Scholl, D. W., Kirby, S. H. & Platt, J. P.) 195–214 (Am. Geophys. Un., 1996).
4. O'Neill, C., Jellinek, A. M. & Lenardic, A. Conditions for the onset of plate tectonics on terrestrial planets and moons. *Earth Planet. Sci. Lett.* **261,** 20–32 (2007).
5. Hyndman, R. D. & Peacock, S. M. Serpentinization of the forearc mantle. *Earth Planet. Sci. Lett.* **212,** 417–432 (2003).
6. Bostock, M. G., Hyndman, R. S., Rondenay, S. & Peacock, S. M. An inverted continental Moho and serpentinization of the forearc mantle. *Nature* **417,** 536–539 (2002).
7. Kawakatsu, H. & Watada, S. Seismic evidence for deep-water transportation in the mantle. *Science* **316,** 1468–1471 (2007).
8. Kao, H. *et al.* A wide depth distribution of seismic tremors along the northern Cascadia margin. *Nature* **436,** 841–844 (2005).
9. Shelly, D. R., Beroza, G. C. & Ide, S. Low-frequency earthquakes in Shikoku, Japan, and their relationship to episodic tremor and slip. *Nature* **442,** 488–491 (2006).
10. Wang, Z., Zhao, D., Mishra, O. P. & Yamada, A. Structural heterogeneity and its implications for the low frequency tremors in Southwest Japan. *Earth Planet. Sci. Lett.* **251,** 66–78 (2006).
11. Nicholson, T., Bostock, M. G. & Cassidy, J. F. New constraints on subduction zone structure in northern Cascadia. *Geophys. J. Int.* **161,** 849–859 (2005).
12. Yuan, X. *et al.* Subduction and collision processes in the central Andes constrained by converted seismic phases. *Nature* **408,** 958–961 (2000).
13. Abers, G. A., van Keken, P. E., Kneller, E. A., Ferris, A. & Stachnik, J. C. The thermal structure of subduction zones constrained by seismic imaging: Implications for slab dehydration and wedge flow. *Earth Planet. Sci. Lett.* **241,** 387–397 (2006).
14. Zandt, G. & Ammon, C. J. Continental crust composition constrained by measurements of crustal Poisson's ratio. *Nature* **374,** 152–154 (1995).
15. Zhu, L. & Kanamori, H. Moho depth variation in southern California from teleseismic receiver functions. *J. Geophys. Res.* **105,** 2969–2980 (2000).
16. Christensen, N. I. Poisson's ratio and crustal seismology. *J. Geophys. Res.* **101,** 3139–3156 (1996).
17. Christensen, N. I. Serpentinites, peridotites, and seismology. *Int. Geol. Rev.* **46,** 795–816 (2004).
18. Rondenay, S., Abers, G. A. & van Keken, P. E. Seismic imaging of subduction zone metamorphism. *Geology* **36,** 275–278 (2008).
19. Moore, J. C. & Vrolijk, P. Fluids in accretionary prisms. *Rev. Geophys.* **30,** 113–135 (1992).
20. Christensen, N. I. Pore pressure and oceanic crustal seismic structure. *Geophys. J. R. Astron. Soc.* **79,** 411–423 (1984).
21. Kodaira, S. *et al.* High pore fluid pressure may cause silent slip in the Nankai Trough. *Science* **304,** 1295–1298 (2004).
22. Gerver, M. & Markushevitch, V. Determination of a seismic wave velocity from the travel time curve. *Geophys. J. R. Astron. Soc.* **11,** 165–173 (1966).
23. Wielandt, E. in *Seismic Tomography* (ed. Nolet, G.) 85–98 (Reidel, 1987).
24. Fisher, A. T. Permeability within basaltic oceanic crust. *Rev. Geophys.* **36,** 143–182 (1998).
25. Caine, J. S., Evans, J. P. & Foster, C. B. Fault zone architecture and permeability structure. *Geology* **24,** 1025–1028 (1996).
26. Kato, A., Sakaguchi, A., Yoshida, S. & Mochizuki, H. Permeability measurements and precipitation sealing of basalt in an ancient exhumed fault of a subduction zone. *Bull. Earthq. Res. Inst. Univ. Tokyo* **78,** 83–89 (2003).
27. Meneghini, F. & Moore, J. C. Deformation and hydrofracturing in a subduction thrust at seismogenic depths: The Rodeo Cove thrust zone, Marin Headlands, California. *Geol. Soc. Am. Bull.* **119,** 174–183 (2007).
28. Ramachandran, K., Dosso, S. E., Spence, G. D., Hyndman, R. D. & Brocher, T. M. Forearc structure beneath southwestern British Columbia: A three-dimensional tomographic velocity model. *J. Geophys. Res.* **110,** B02303 (2005).
29. Ahrens, T. J. & Schubert, G. Gabbro–eclogite reaction rate and its geophysical significance. *Rev. Geophys.* **13,** 383–400 (1975).
30. Coleman, R. G. Petrologic and geophysical nature of serpentinites. *Geol. Soc. Am. Bull.* **82,** 897–918 (1971).

Supplementary Information is linked to the online version of the paper at www.nature.com/nature.

Acknowledgements We thank E. Davis and M. Jellinek for discussions. Data used in this study come from the Canadian National Seismological Network and are distributed freely by the Geological Survey of Canada.

Author Contributions P.A. and M.G.B. designed the study, analysed the data and wrote the paper; N.I.C. and S.M.P. participated in the interpretation of results.

Author Information Reprints and permissions information is available at www.nature.com/reprints. Correspondence and requests for materials should be addressed to P.A. (paudet@berkeley.edu).